Structure of Latex−Silica Nanocomposite Films: A Small-Angle Neutron Scattering Study

Julian Oberdisse*,† and Bruno Demé‡

Laboratoire Léon Brillouin, CEA/CNRS, CEA Saclay, 91191 Gif sur Yvette Cedex, France, and Institut Laue-Langevin, 6, rue Jules Horowitz, BP 156, 38042 Grenoble Cedex 9, France

Received October 23, 2001

ABSTRACT: We report on the synthesis and structure of silica-filled latex films. The main stage of the synthesis consists of physicochemical manipulations of colloidal solutions of nanosilica and nanolatex beads, followed by drying and filmification. Hence, no mechanical energy which might contribute to building or destruction of aggregates of silica beads is supplied to the samples.We have analyzed the structure of the resulting filled latex films by means of small-angle neutron scattering. The scattered intensity varies enormously with the physicochemical parameters, indicating considerable structural modifications. To rationalize these results, we present a unified description of the data which successfully accounts for the main characteristics of the scattered intensity: the form factor of beads at large q vectors, the position of the intra- and interaggregate structure factor peaks, the small-q upturn observed in some cases, and the overall intensity in absolute units. This allows us to quantify the degree of aggregation of the silica in the matrix. It is found that the latter can be varied in a systematic manner by changing pH, silica volume fraction, and quantity of added salt. In one extreme case, for example, the aggregation number changes by a factor of about 1000 at constant silica volume fraction.

I. Introduction

Elastomers filled with small and hard particles are of great importance for the rubber industry, where carbon black and silica are commonly used fillers.[1−6] These improve the mechanical properties of polymeric material like the elastic modulus or resistance to abrasion. This reinforcement of polymers has been studied in the past from many different points of view, by experiment, theory, and simulation. The wealth of approaches seems to be due to the complexity of reinforcement, where effects on different length scales interact. Some studies focus on chain conformation and dynamics, and changes induced by the presence of filler,[7−13] others on the interactions at the filler surface,[14−18] and again others on interactions between fillers and the large-scale structure of the filler in the polymeric matrix ("filler networking").[19−28] Moreover, nonspherical fillers like fibers or disks or special filler surface treatments can further increase the complexity.[2,3,16,29−31]

In this article, we present the first part of a study of the relationship between the filler structure and the rheological properties of a model nanocomposite material. It consists of (hard) nanosilica spheres embedded in a soft polymeric matrix, which is itself formed from nanolatex particles. Strictly speaking, the matrix is an entangled melt and not a rubber; i.e., there are only transient junctions between chains. At the temperature of interest, however, the flow of the material is sufficiently slow, and the observed reinforcement effects are sufficiently strong that our conclusions are nonetheless relevant for filled rubber as well. Our system is solvent cast; i.e., it is controlled by physicochemical manipulations in solution, which has a variety of advantages: (a) No mechanical mixing or mechanical energy input is needed for its preparation. (b) The processes governing latex film formation are now well understood.[32−34] (c) Silica is a lot harder than the matrix polymer. The system represents thus an important limiting case of practical relevance. (d) The Silica−latex−surface interactions are always the same, independent of the structure of the filler. (e) The constituents, latex and silica particles, can be studied individually. (f) The system has a high contrast for small-angle neutron scattering (SANS) experiments.

In section II, we present experimental details about the synthesis of the nanocomposite films as well as about the SANS experiments and data analysis. In section III, we turn to a SANS study of the individual components (latex and silica beads) and the structure of nanolatex−silica films obtained in various physicochemical conditions. Results are discussed in the last section, where we rationalize the data in terms of the aggregation number of silica in the matrix. In a forthcoming article we will confront the measured filler structure with the mechanical properties tested in uniaxial elongation.

II. Experimental Section

II.1. Sample Preparation. The colloidal silica samples Bindzil B30/220 and Bindzil B40/130 were a gift from Akzo Nobel, Sweden. The aqueous solution of $c = 30$ wt % for B30 (40 wt % for B40) was initially at pH 9. They were diluted to $c = 10$ wt %, deionized by means of an ion-exchange resin and filtered with a Millipore Steril Filter (0.8 μm). The resulting conductivity of the stock solutions was of the order of 100 μS/cm, at pH between 3 and 4. By immediate addition of small quantities of NaOH (1.0 M), the pH was adjusted to the desired value and the colloidal stability was preserved. The average size given by Akzo Nobel is $R = 75$ Å for B30 and $R = 125$ Å for B40. The polydispersity is expected to be important.

The nanolatex was kindly provided by Rhodia. It is a core−shell latex of poly(methyl methacrylate) (PMMA) and poly(butyl acrylate) (PBuA), with a hydrophilic shell containing methacrylic acid. This hydrophilic shell is known to be less well-defined than shells of bigger latex particles:[26] The surface

† CEA/CNRS.
‡ Institut Laue-Langevin.
* Author for correspondence.

10.1021/ma0118419 CCC: $22.00
Published on Web 04/17/2002

is simply enriched in methacrylic acid in order to ensure the colloidal stability in water. The key parameter for mechanical measurements is the glass transition temperature of the core: $T_g = 33$ °C. The initial concentration of nanolatex was 30 wt %, at pH 9, and it has been processed in the same way as the colloidal silica. The approximate size given by Rhodia is $R = 200$ Å.

Samples were prepared by mixing appropriate amounts of silica and latex stock solutions (previously brought to the desired pH) in order to obtain a given volume fraction Φ of silica in the final composite film. Note that addition of NaOH changes both the pH and the conductivity L_s. In some experiments, NaCl (between 0.01 and 0.25 M) was added to the aqueous mixture to further increase the conductivity without changing the pH. Solutions were degassed in primary vacuum for several hours at room temperature and then cast into preheated Teflon molds of dimensions 4×4 cm^2 or 5×5 cm^2. Film formation takes about 4 days at 65 °C, and bubble-free, transparent, sometimes slightly yellowish and homogeneous films of 1−2 mm thickness were obtained.[32−34] These were further smoothed with sandpaper in order to achieve constant thickness, which is important for the calibration of the scattered intensity.

II.2. Small-Angle Neutron Scattering. Experiments have been performed at LLB on beamline PACE and at ILL on beamline D11. Here we report mainly on the D11 experiment. The wavelength was fixed to 10.0 Å, and the sample-to-detector distances were 1.25, 3.50, 10.00, and 36.70 m, with corresponding collimation distances of 5.50, 5.50, 10.50, and 40.00 m, respectively. On spectrometer PACE, two configurations were used: a first one with wavelength 9.3 Å, sample-to-detector distance of 4.58 m, and a collimation distance of 5.00 m, and a second one with wavelength 5.1 Å, sample-to-detector distance of 1.13 m, and a collimation distance of 2.50 m. Data treatment has been done with a homemade program following standard procedures,[35,36] with H_2O as calibration standard. D11 spectra from different configurations superimpose almost perfectly due to the common wavelength implying the same (weak) contribution of inelastic, incoherent, and multiple scattering. Small deviations found in the spectra at the overlap of two configurations are due to different resolution conditions. For absolute intensities in cm^{-1}, the incoherent scattering cross section of H_2O was estimated from a measurement of the attenuator strength and of the direct beam with the same attenuator. The incoherent scattering background of the nanocomposite samples was subtracted by enforcing a high-q Porod ($I = Aq^{-4}$) behavior, which is known to be present from calibration measurements with individual silica beads. The latter are the main building blocks of the nanocomposites and have therefore been analyzed by fitting theoretical spectra, which take polydispersity into account and which are convoluted for each configuration with the corresponding resolution function, calculated according to Lairez.[37] This includes the angular resolution due to the finite collimation, the detector cells, and the wavelength spread of 9% of the mechanical velocity selector.

II.3. Modeling the Scattered Intensity. The scattering from interacting aggregates formed of polydisperse spheres is easily described for isotropic structures with small polydispersity in the number of aggregation N_{agg}. The differential scattering cross section per unit volume $I = d\Sigma/d\Omega$ can then be written in a good approximation as the product of an interaggregate structure factor $S_{agg}(q)$ and a normalized aggregate form factor $F^2_{agg}(q)$:[36,38,39]

$$I(q) = \Phi \Delta\rho^2_{si-la} V_{agg} S_{agg}(q) F^2_{agg}(q) \quad (1)$$

where $\Delta\rho_{si-la}$ is the contrast, i.e., the difference in scattering length density between silica and the polymer matrix. V_{agg} is the average scattering volume of an aggregate due to silica beads only. In the presence of liquidlike order between aggregates, $S_{agg}(q)$ has a correlation peak at $q_0 = 2\pi\alpha/D$, where D is the average distance between aggregates and α is a parameter reflecting the degree and type of positional order of the aggregates. The position of the peak gives an estimation of the mean aggregation number:

$$N_{agg} \approx D^3 \Phi / V_{si} \quad (2)$$

where the silica volume fraction Φ and average volume of a silica sphere V_{si} are known. The model used to derive eq 2 is to place all aggregates on a cubic lattice of periodicity D, thus set α to 1, and apply the conservation of silica volume on a unit cell. Without a precise knowledge of α, one can only give a rough estimate of N_{agg}, due to the liquidlike order of the samples. A better description of this order would lead to a numerical prefactor $\alpha > 1$; i.e., we typically underestimate aggregation numbers by some factor α^3 between 1.2 and 2. Note that eq 2 implicitly assumes that there is no higher order clustering, i.e., that the aggregates are homogeneously distributed in space.

$F^2_{agg}(q)$ in eq 1 is a decreasing function of q in the small-q range, starting from 1 with a decay typical for the form and size of the aggregate. The Guinier approximation holds at small angles ($qR_g \ll 1$):

$$F^2_{agg}(q) = e^{-q^2 R_g^{2/3}} \quad (3)$$

where R_g is the radius of gyration of the aggregate. The aggregate form factor can be decomposed into an intraaggregate structure factor and the form factor of the silica spheres:

$$V_{agg} F^2_{agg}(q) = V_{si} S_{intra}(q) F^2_{si}(q) \quad (4)$$

$F^2_{si}(q)$ is the normalized form factor of a silica sphere. S_{intra} is the intraaggregate structure factor, and it corresponds to the correlations between the centers-of-mass of the silica spheres making up an aggregate. Its small angle value $S_{intra}(q \to 0)$ is N_{agg}, and it tends toward 1 at large q values. $S_{intra}(q)$ can be calculated by numerical simulation, the input being the size distribution of the silica spheres and an appropriate building rule for the aggregate.[40,41]

In the absence of position correlations between aggregates (high dilution, $S_{agg}(q) = 1$), one can take polydispersity in aggregation number into account by summing the different contributions. An example of bidispersity will be discussed below.

III. Results

III.1. Scattering from Isolated Spheres. The scattering length density of macroscopic silica (SiO_2) is $\rho_{si} = 3.5 \times 10^{10}$ cm^{-2}, while typical values for hydrogenated polymers lie around 1×10^{10} cm^{-2}. For the colloidal silica and nanolatex this was confirmed by external contrast variation in H_2O/D_2O mixtures ($\rho_{NL} = 0.9 \times 10^{10}$ cm^{-2}). The form factor of the silica particles $F^2_{si}(q)$ was measured in a highly diluted (0.12 vol %) solution in D_2O to suppress the contribution of the interparticle structure factor. The spectra $I(q)$ are shown in Figure 1. They have the typical shape of scattering from polydisperse objects; i.e., they present some oscillations reminiscent of form factor oscillations. They have been analyzed in the following manner: the limiting scattered intensity at zero angle $I(q \to 0)$ and the equivalent sphere radius $R_{Guinier}$ were read of from a ln $I(q)$ vs q^2 plot. Together with the Porod constant A from the high-q tail, one can determine the polydispersity, the average radius, and the contrast (cf. Appendix A for details). For B30, the scattering can thereby be shown to be consistent with a log-normal radius distribution function (see fits[46] in Figure 1) of spheres with parameters $R_0 = 76.9$ Å, with a polydispersity in radius of $\sigma = 0.186$ and a contrast of 2.7×10^{10} cm^{-2}. The latter value is exactly what one expects from the solvent (D_2O and some H_2O

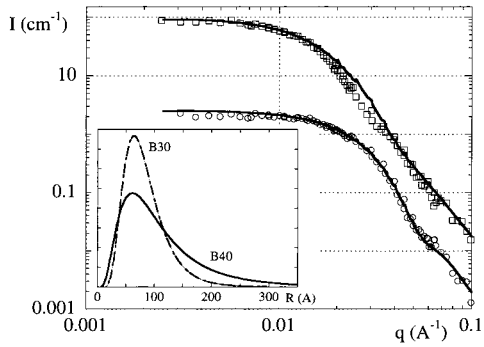

Figure 1. Scattered intensity I in cm^{-1} as a function of scattering wave vector q in Å^{-1} from dilute solutions of B30 (circles) and B40 silica (squares, $I(q)$ multiplied by 10 for clarity). The fits include a log-normal size distribution (shown in the inset) and the resolution function of the spectrometer. The parameters are listed in Table 1.

Table 1. Characterization of Colloidal Samples[a]

	ρ (10^{10} cm^{-2})	$R_{Guinier}$ (Å)	R_p (Å)	R_0 (Å)	σ	V (10^6 Å^3)
B30	3.5	98	83.8	76.9	0.186	2.23
B40	3.3	160	113.8	92.6	0.279	4.72
nanolatex	0.9	210	152.7	138.9	0.243	14.64

[a] ρ is the scattering length density. R_0 and σ are the parameters of the log-normal distribution used to fit the scattering curves of dilute solutions. V is the average volume of a bead. R_p and $R_{Guinier}$ are defined in Appendix A.

from the silica colloidal solution) scattering length density of 6.2×10^{10} cm^{-2}. Note also that the Schultz−Flory distribution gives equivalent results, whereas the Gaussian is less satisfactory, presumably due to the absence of a tail. For B40, the parameters are $R_0 = 92.6$ Å, with a polydispersity in radius of $\sigma = 0.279$ and a contrast of 2.9×10^{10} cm^{-2}, which is also reasonably close to the calculated value. Both distribution functions are shown in the inset of Figure 1. An equivalent treatment of the nanolatex yields an average radius of $R_0 = 138.9$ Å, a polydispersity of $\sigma = 0.243$, and a scattering length density of 0.9×10^{10} cm^{-2}. The data show that our particles are relatively well-defined and not aggregated. This demonstrates also the absence of aggregation in the stock solutions used to produce the nanocomposite films, the samples for the data shown in Figure 1 having been prepared *after* the film samples. All data on colloidal particles are summarized in Table 1.

III.2. Scattering from Nanocomposite Films. We present here some representative results, which show a systematic variation with the different physicochemical parameters. Among these, pH and volume fraction induce the largest and most interesting changes. The samples in some of the series in volume fraction are made with the bigger silica beads (B40), to test the influence of the size ratio with respect to the latex spheres. The average radius $\langle R \rangle$ of the silica (B30 and B40) particles is a bit more than one-half and about two-thirds of the radius of the nanolatex, respectively, a small but significant change which allows us to study the influence of the size on the packing and aggregation behavior of the silica spheres during film formation.

a. Effect of pH. Samples from solutions with six different values of pH have been made, from 3.9 to 9.1, with silica particles B30 at a fixed volume fraction $\Phi =$ 5.0% and without added salt. In Figure 2 we show the intensity I as a function of scattering vector q in a

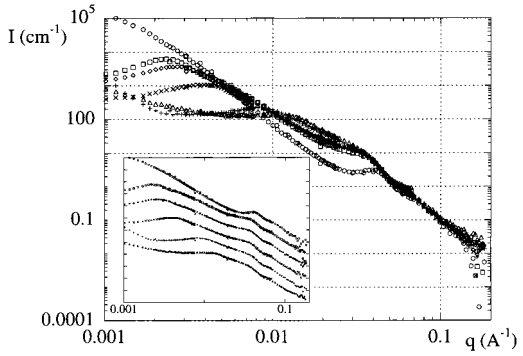

Figure 2. Scattered intensity I in cm^{-1} as a function of scattering wave vector q in Å^{-1} from nanocomposites films of silica B30 at fixed volume fraction $\Phi = 5.0\%$, for different pH values, no added salt: (○) pH 3.9, (□) pH 5.1, (◇) pH 6.0, (×) pH 7.0, (+) pH 8.0, (△) pH 9.1. In the inset the same data are shown, with the intensities multiplied by powers of 10, starting at low pH.

double-logarithmic presentation. The same data are represented in the inset of Figure 2, with the intensity multiplied by powers of 10, starting at low pH (i.e., pH 3.9 unchanged). Let us first describe the curves qualitatively. All of them superimpose at large q, and in the intermediate q range, around $(3-4) \times 10^{-2}$ Å^{-1}, all curves display a shoulder (or even a maximum for pH 3.9). The low-q intensity increases considerably as the pH decreases, up to very high values (10^5 cm^{-1} at $q = 10^{-3}$ Å^{-1} for pH 3.9), which possibly indicate some multiple scattering. Besides the sample made from the most acid solution, the curves show a maximum with a high intensity at low q, and the position of this maximum shifts toward higher q as the pH increases. Note that the two samples made from the most basic solution have also a small-q upturn. We will see later that this is systematic for all "basic" samples.

Let us translate these trends in direct space: the more acid the conditions of synthesis, the larger the aggregates formed by the silica. This explains both the overall increase of the intensity, which is roughly proportional to the mass of individual aggregates, and the shift in the low-q maximum. In this picture, the latter corresponds to a distance between these aggregates, which is larger when the aggregates are larger, at constant volume fraction. Let us check this model. From eq 3 one sees that the typical range of the decay of $F^2(q)$ is of the order of $1/R_g$, the exact form of F^2 being not of importance here. The argument is the following: if one changes the scale of the system without changing the compacity of the aggregates or the type of interaction between them, then a scaling law should relate the intensity $I(q_0)$ of the low-q maximum to its position q_0:

$$I(q_0)^{1/3} = \beta/q_0 \tag{5}$$

where β is some constant of proportionality. Physically, blowing up the system at constant silica volume fraction means increasing the distances and sizes by some factor while increasing the volume of aggregates and thus the overall intensity by the same factor cubed. The plot of $I(q_0)^{1/3}$ vs $1/q_0$ is shown in Figure 3. The linear relationship is quite well fulfilled. One can conclude that our picture in real space of the aggregation is correct. Moreover, the interaction between aggregates and their compacity do not change much as the pH changes; i.e.,

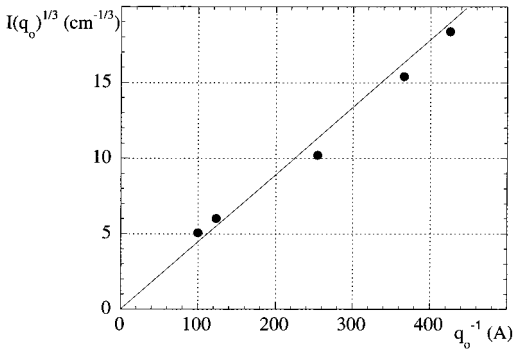

Figure 3. Low-q maximum intensity $I(q_0)^{1/3}$ (in $cm^{-1/3}$) vs $1/q_0$ (in Å) for the data shown in Figure 2. The line is a guide to the eye. See text for details.

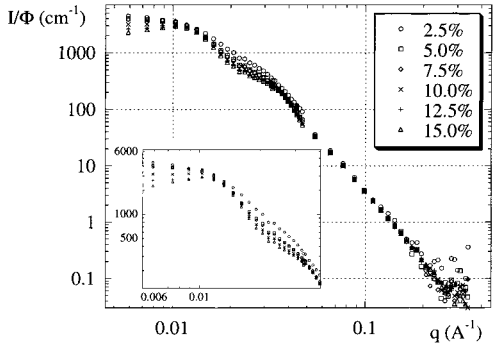

Figure 4. Relative scattered intensity I/Φ in cm^{-1} as a function of scattering wave vector q in $Å^{-1}$ from nanocomposites films of silica B30 at fixed pH = 9.0, for increasing volume fraction Φ, no added salt. In the inset a close-up of the low-q region is shown.

the product $S_{agg}(q_l)F^2_{agg}(q_0)$ remains approximately constant when increasing the size of the aggregates. We will further discuss this point in section IV.

The other feature of the scattering curves is the shoulder in the intermediate q range which is more and more pronounced as pH increases. Its abscissa is independent of the system and must thus be due to a distance between elementary silica particles, at $q \approx 2\pi/2R = 0.04$ $Å^{-1}$, in good agreement with the observed position of the shoulder. Its enhancement can be understood because in bigger aggregates there are more and more directly neighboring beads.[40] We now turn to a detailed study of the influence of Φ.

b. Effect of Silica Volume Fraction and of the Silica/Latex Size Ratio. The structure of nanocomposite films of increasing silica (B30) volume fraction Φ, without added salt and at constant pH = 9.0, has been studied. The series of spectra corresponding to Φ = 2.5%, 5.0%, 7.5%, 10.0%, 12.5%, and 15.0% has been measured on instrument PACE (LLB). They are shown in Figure 4 in $I(q)/\Phi$ representation. The spectra superimpose well at higher wave vector and show some characteristic differences at smaller wave vectors. In the inset of Figure 4, we plot the low-q part of the data. At low volume fractions (Φ < 7.5%) the spectra show only a soft shoulder at $q \approx 0.01$ $Å^{-1}$ instead of the low-q maximum described above (cf. Figure 2). At these rather low Φ, the interaggregate structure factor is thus too weak to be clearly visible in the spectra. The position of the shoulder, however, is approximately stable with the volume fraction.[47] At higher Φ (10.0%, 12.5%, and 15.0%), the shoulder evolves into a low-q interaggregate correlation peak. Its position q_0 is shifted to slightly

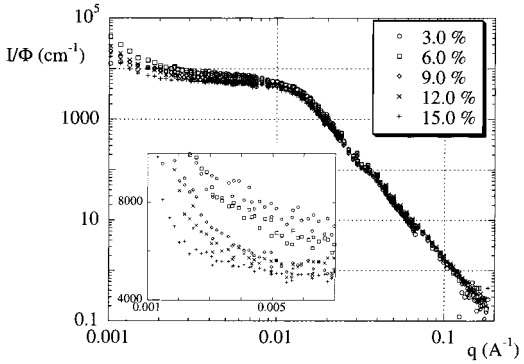

Figure 5. Relative scattered intensity I/Φ in cm^{-1} as a function of scattering wave vector q in $Å^{-1}$ from nanocomposites films of silica B40 at fixed pH = 9.0, for increasing volume fraction Φ, no added salt. In the inset a close-up of the plateau region is shown, in linear scale.

higher q values, and we will see in the discussion that this can be translated by a roughly constant number of aggregation. In other words, as the volume fraction increases, there is creation of new aggregates, all more or less of the same size. Two other general features of these spectra are that the relative intensity $I(q)/\Phi$ in the range of the peak is lower for higher volume fractions and the presence of a small-q upturn.

The structure of nanocomposite films made up of the same nanolatex but of larger silica spheres (B40, characterized in section III.1) has been studied in analogous series in volume fraction, at pH 9.0: Φ = 3.0%−15.0%. The spectra, measured on D11, are shown in Figure 5 in $I(q)/\Phi$ representation. The good superposition of the spectra in this representation is striking. Apart from the standard high-q behavior, which superimposes again well, the main features are the small-q upturn, followed (in q) by a plateau around $q = 0.005$ $Å^{-1}$ up to a shoulder around $q = 0.01$ $Å^{-1}$.

In Figure 5, the *small-q upturn* is probably due to a few large aggregates, which do not contribute to the scattering at higher angles. It is difficult to describe the scattering from these big aggregates, as both their number and their size are unknown. Moreover, the information contained in the spectra is incomplete due to the limited q range. To extract at least estimations of the number of big aggregates from the measured intensity, we propose in Appendix B a simple model which relies on an assumption of the functional form of the aggregate form factor. This allows us to estimate the product of the number and of the size of the big aggregates from the shape and the position of the upturn. Following these calculations, less than 10% of all silica beads are contained in the large aggregates, which have numbers of aggregation of the order of several hundreds.

The next interesting feature is that the *relative intensities* I/Φ *at the plateau* are again in inverse order, i.e., highest for Φ = 3.0%, just like in the data series with silica B30. This is shown in the inset of Figure 5. We interpret this as another hint in favor of the picture of very few large aggregates coexisting with individual beads. Indeed, as the size of the big aggregates grows with increasing volume fraction, they scatter more and more at small angles (the small-q upturn, described by the increasing radius of gyration) and scatter thus less at intermediate angles. In Table 2 we report the values of I at the plateau, and we compare them to the theoretical values I^{theo} at the same wave vector ($q \approx$

Table 2. Observed Plateau Intensity (in cm^{-1}) for the Series in Volume Fraction Φ, Silica B40 and pH 9.0[a]

series in Φ: B40 pH 9	$I_{plateau}$ (cm^{-1})	I_{theo} ($q \approx 0.006$ Å^{-1}) (cm^{-1})	N_{agg}
Φ = 3.0%	230	146	1.6
Φ = 6.0%	400	293	1.4
Φ = 9.0%	515	439	1.2
Φ = 12.0%	635	586	1.1
Φ = 15.0%	810	732	1.1

[a] It is compared to the theoretical intensity for individual beads at the same volume fraction and under identical contrast conditions. The average aggregation number is estimated through the ratio of the two intensities. It reflects the fact that the majority of the beads are individual beads.

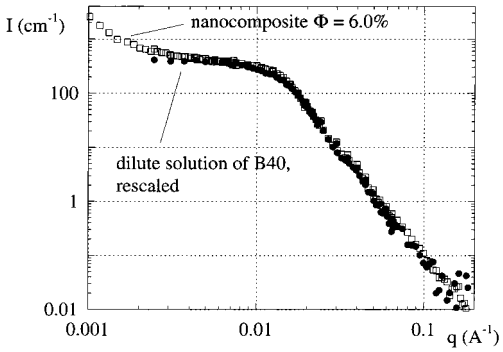

Figure 6. Comparison of scattered intensity I in cm^{-1} as a function of scattering wave vector q in Å^{-1} of a nanocomposites film (silica B40, pH = 9.0, Φ = 6.0%) and of the dilute solution of B40, rescaled by the appropriate factor; see text for details.

0.006 Å^{-1}) for individual spheres. The agreement is quite remarkable and leads us to the following conclusion: in this system, at pH 9.0, increasing the concentration does not increase the number of aggregation of the majority of beads, which coexist with rare but quite large aggregates. The ratio of the intensities gives an estimation of the average aggregation number N_{agg}, which is of the order of 1 (cf. Table 2). In short, beads stay individual beads, in the whole range of volume fractions under examination (Φ = 3.0−15.0%). To cross-check this result, we have superimposed in Figure 6 a typical spectrum of the series (Φ = 6.0%) with the form factor of the individual beads. In this case, the scattered intensity is proportional to the number of aggregation, the volume fraction of scattering objects, and the square of their contrast with the matrix. To account for the difference in aggregation ($N_{agg} = 1.4$, cf. Table 2), volume fraction (Φ = 0.12% of B40 in the solution and 6.0% of B40 in the film), and contrast conditions ($\Delta\rho_{solvent-si} = 2.9 \times 10^{10}$ cm^{-2}, $\Delta\rho_{si-la} = 2.4 \times 10^{10}$ cm^{-2}, cf. Table 1), the intensity of the colloidal solution has been multiplied by the appropriate constant $1.4 \cdot (6.0/0.12) \cdot (2.4/2.9)^2$.

The agreement gives further credibility to our interpretation of the data, especially because the last important feature, the *shoulder*, is very nicely reproduced. Note that this works equally well with other samples of the series, whereas the analogous superposition is not possible in the B30 series, indicating higher numbers of aggregation there. As a last point, we would like to mention that the structure factor between individual beads should have its maximum in the zone between q = 0.01 and 0.02 Å^{-1}, where it is too weak to be detected in the overall decrease of the intensity.

We now report on a series in silica (B40) volume fraction at constant pH = 5.0, i.e., under conditions where a rather high aggregation is expected. The

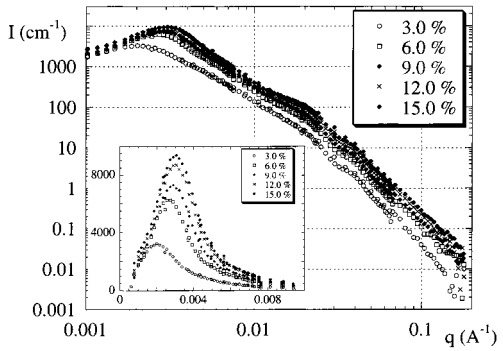

Figure 7. Scattered intensity I in cm^{-1} as a function of scattering wave vector q in Å^{-1} from nanocomposites films of silica B40 at fixed pH = 5.0, for increasing volume fraction Φ, no added salt. In the inset the low-q intensity is shown in linear scale.

spectra are plotted in Figure 7. As was the case with the other spectra discussed before, the high-q part is simply the form factor of the silica beads and would superimpose well in $I(q)/\Phi$ representation. In the low-q part, a very prominent maximum can be seen. In the inset of Figure 7, we present the data in linear form, which emphasizes this main peak. With increasing volume fraction, from 3.0% to 15.0%, the intensity increases considerably, and the peak shifts from q_0 = 0.0020 to 0.0030 Å^{-1}. The intensities are very high, indicating strong aggregation. It is interesting to note that $I(q)/\Phi$ has again an inverted order in the intensity at the peak; i.e., the sample with Φ = 3.0% has the highest relative peak intensity $I(q_0)/\Phi$, almost a factor of 2 higher than the 15.0% sample. This result is particularly striking in the presence of a structure factor peak; it can be explained by the same type of argument as in the previous series. There the decrease of the relative plateau intensity I/Φ could be traced back to the growth of some big aggregates. Here we have only big aggregates, and in the discussion we will show through a simulation of the corresponding intraaggregate structure factor $S_{intra}(q)$ that the picture is correct.

c. Effect of Added Salt. We have investigated the effect of monovalent salt (NaCl) on the structure of the silica−polymer nanocomposites. Salt screens the stabilizing electrostatic repulsion between colloidal particles, and addition of high amounts leads to flocculation of the solution. Small quantities of salt, however, may change the range of the electrostatic interaction without destabilizing the colloid. Changes in the resulting aggregate structure (after filmification) are therefore to be expected. To study this, we have measured the intensity scattered from four films with different conductivities L_s = 450 (no added salt), 550, 725, and 1050 μS/cm. All four have the same volume fraction of silica B30 (Φ = 15.0%) and a pH of 9.0 in order to start from a system with initially little aggregation. The results are shown in Figure 8, with the intensities multiplied by powers of 10 for clarity (lowest L_s data unchanged). The scattering curves can be interpreted along the same lines as the pH series discussed above. The high-q scattering is identical, and data can be brought to perfect superposition there (not shown). The low-q structure peak moves very slightly to the left with increasing salinity (this is visible in linear scale) and disappears completely for the highest salinity. Although we have only a few data points, one can test the simple scaling law, eq 5: from L_s = 450 mS/cm to L_s = 725 mS/cm the peak shift indicates an increase in V_{agg} by a

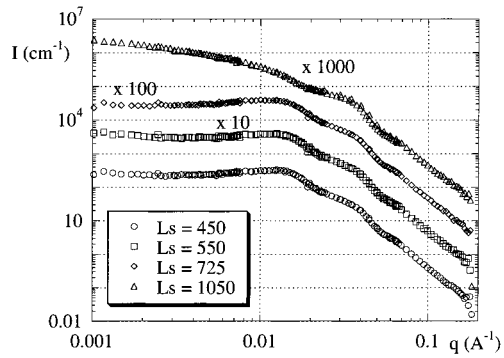

Figure 8. Scattered intensity I in cm^{-1} as a function of scattering wave vector q in $Å^{-1}$ from nanocomposites films of silica B30 at fixed volume fraction $\Phi = 15.0\%$, fixed pH = 9.0, for different conductivities L_s in μS/cm. The intensities are multiplied by powers of 10, starting at low L_s.

factor 1.5, which is not followed by the peak height. The latter increases only a factor of 1.2, and we have two ways of interpreting this: either the interaggregate structure factor weakens due to screening, or the aggregates become less compact (higher R_g), or both. As the screening due to salt may influence both the inter- and intraaggregate correlations, both hypotheses seem reasonable, and a detailed modeling of the aggregate structure and interaction would be necessary to solve this issue. What is sure is that the aggregation number increases by 50% when adding salt up to 725 mS/cm, and above 725 mS/cm the aggregation (or even flocculation) increases too much to be followed by SANS.

IV. Discussion in Terms of Aggregation Numbers

We have seen in section III that the scattering from the model nanocomposite films varies considerably with the physicochemical conditions in solution before film formation. Physically, this is due to the fact that the equilibrium between attractive, short-ranged van der Waals forces and long-ranged electrostatic repulsion is modified by, e.g., addition of salt. The effect of pH is more subtle, as it affects both the colloidal charge and the screening length. Under low-pH conditions or high salt content, the colloidal stability is weakened. Even if the suspension is still stable at the beginning of the drying process, it will eventually become unstable as the concentration of ions increases also during drying. This instability favors aggregation which competes with the coalescence of the latex beads. These form a continuous matrix and finally freeze the aggregation of silica. Thus, the modification of the interactions in solution leads to a different organization of the silica in the final film, after evaporation.

The scattering from our nanocomposite films can be understood using the tools given in eqs 1−4, and a coherent description has been obtained. In particular, as we have seen in section II, aggregation numbers can be deduced from a simple cubic lattice model, eq 2. Keep in mind that they are estimations ($\alpha = 1$) and that higher-level clustering cannot be completely ruled out due to the limited q range. However, they can be compared among each other because the type of order is not expected to be changed fundamentally from one sample to the next (no colloidal crystallization). Of course, the aggregation numbers are estimated with higher precision in the presence of a well-defined peak than with a soft shoulder. We summarize all our results in Tables 3−6.

Table 3. Estimation of the Average Aggregation Number through the Position of the Structure Factor Peak for the Series in pH, Silica B30, at $\Phi = 5.0\%$[a]

series in pH: B30, $\Phi = 5.0\%$	agg no. ($\alpha = 1$)	slope at intermediate q	small-q upturn
3.9	>5500	$I \propto q^{-3.8}$ over a decade	no
5.1	429	$I \propto q^{-2.9}$	no
6.0	273	$I \propto q^{-2.8}$	no
7.0	92	$I \propto q^{-2.6}$	no
8.0	10	$I \propto q^{-2.5}$	yes, $I \propto q^{-3.3}$ in short q−range
9.1	4−8	$I \propto q^{-2.5}$	yes, $I \propto q^{-1.5}$

[a] The slope at intermediate angles ($q > q_0$, the position of the structure factor peak), gives the fractal dimension of the aggregates. The small-q upturn can be attributed to the presence of very few, big aggregates. For the most "acid" sample, a lower bound of the aggregation number is deduced from the absence of the peak.

The series in pH (cf. Table 3) presents the most striking changes in structure. At high pH, the number of aggregation is in the range from 4 to 8, whereas a lower bound of several thousand is found at low pH. Let us discuss the structure of the most "acid" sample, where a lower bound of the aggregation number is deduced from the absence of the peak: if it exists, q_0 is outside the accessible q range: $q_0 < 10^{-3}$ Å $^{-1}$. We obtain the estimation of the aggregation number $N_{agg} > 5500$, which in turn would give a scattered intensity of isolated aggregates for $I(q \rightarrow 0)$ of more than 5×10^5 cm^{-1}. Because of the many unknown variables of the system like the aggregate geometry (eq 3) and the interaggregate structure factor, it is no longer possible to make any precise estimation. It is encouraging, however, that the magnitude of the scattered intensity is of the same order as our estimation. Moreover, the data follows a power law which is very close to q^{-4} over a large range *at low q*, indicating very compact aggregates. Note that this agrees with our interpretation of the peak at $q \approx (3-4) \times 10^{-2}$ $Å^{-1}$ (effect of pH, section III.2). At this q value, the other samples, at higher pH, have only a shoulder. The fractal dimension of these aggregates is also reported in Table 3. As one can see, the fractal dimension decreases from about 2.9 to 2.5 with increasing pH; i.e., the aggregates are less and less compact. This change in compacity and therefore of the intraaggregate structure factor is apparently insufficient to invalidate eq 5, as can be seen in Figure 3, but we cannot exclude that phenomena on bigger length scales, like higher-order clustering, bias the picture.

Like the pH, the quantity of added salt has a direct influence on the final structure of the film, via the Debye screening length. The changes in scattered intensity as a function of the quantity of added salt are much more abrupt, though (cf. Table 4). Initially, the aggregation number stays roughly constant (i.e., below $L_s = 725$ mS/cm), and above this value it is already unmeasurably high; i.e., there is no observable structure factor peak. This suggests that salt destabilizes completely the colloidal solution at some stage of the drying process. We can only guess about the details of this collapse, but it is interesting to see that the resulting structure of the sample with a high quantity of added salt is different from the one at low pH (cf. preceding paragraph): the scattered intensity is a lot weaker, and the low-q scaling of the intensity with q is different. Although there is no clear power-law behavior, the

Table 4. Estimation of the Average Aggregation Number through the Position of the Structure Factor Peak for the Series in Added Salt, Silica B30, at pH 9.0 and Volume Fraction Φ = 15.0 %[a]

series in salinity: B30, Φ = 15.0%, pH = 9	agg no.	small-*q* upturn
450 μS/cm (no added salt)	10	yes
550 μS/cm	15	yes
725 μS/cm	15	yes
1050 μS/cm	unknown, presumably very high	no

[a] The small-*q* upturn can be attributed to the presence of very few, big aggregates.

Table 5. Estimation of the Average Aggregation Number through the Position of the Structure Factor Peak for the Series in Volume Fraction Φ, Silica B30, at pH 9.0[a]

series in Φ: B30, pH = 9.0	agg no.	small-*q* upturn
Φ = 5.0%	4−8	yes
Φ = 10.0%	11	not measured
Φ = 12.5%	12	not measured
Φ = 15.0%	10	yes

[a] The small-*q* upturn and the peak position could not be measured for Φ = 2.5% and 7.5%.

Table 6. Estimation of the Average Aggregation Number through the Position of the Structure Factor Peak for the Series in Volume Fraction Φ, Silica B40, at pH 5.0[a]

series in Φ: B40, pH = 5.0	agg no.	series in Φ: B40, pH = 5.0	agg no.
Φ = 3.0%	188	Φ = 12.0%	238
Φ = 6.0%	168	Φ = 15.0%	292
Φ = 9.0%	196		

[a] No small-*q* upturn is ever observed.

intensity decreases roughly like q^{-1} at $q < 10^{-2}$ Å^{-1}, and not at all like q^{-4}, as in the case of the very low-pH sample. It is tempting to interpret this as scattering from one-dimensional aggregates (chains or long branches), at least at the length scales relevant to the scattering. This agrees also with the less prominent peak at $q \approx (3-4) \times 10^{-2}$ Å^{-1}. In this case there is no possibility to estimate the aggregation number. On a more speculative basis, the power law suggests the formation of some infinite network formed by the silica in the matrix.

Although the results are less spectacular, the series in volume fraction are equally interesting. At high pH (cf. Table 5), there is evidence for the presence of a second, small population of very big aggregates. The aggregation of the silica of the majority of beads does not increase with volume fraction. A comparison of the data from the small and the larger silica beads shows that the smaller silica beads are more aggregated by about a factor of 10.

At low pH (cf. Table 6), no evidence for a second population is found. Instead, the aggregates are a lot bigger, they grow with volume fraction, and the degree of organization of the structure seems very high because of the very pronounced structure factor peak. In the Results section, we have already underlined the fact that the relative peak intensities I/Φ are in inverse order. It is plausible that this is due to the decrease of the intraaggregate structure factor $S_{intra}(q)$ between 0.002 and 0.003 Å^{-1} (B40, pH 5.0). We have used the estimation of the average number of aggregation given in Table 6 as input for a simulation of the $S_{intra}(q)$. In Figure 9, three examples are shown for $N_{agg} = 188$, $N_{agg} = 292$, and $N_{agg} = 400$. Between $q_o = 0.0020$ and 0.0030 Å^{-1} the curves fall steeply, which explains nicely why the peak for Φ = 15% is below the one for Φ = 3% in I/Φ, instead of the higher aggregation number. Indeed, comparing in Figure 9 the value of the curve at the peak position $q_0 = 0.0020$ Å^{-1} for $N_{agg} = 188$ at Φ = 3% to the one at 0.0030 Å^{-1} (the peak position at Φ = 15%) for $N_{agg} = 292$, we find a factor of 2.4. Now, with the change in volume fraction from 3% to 15%, the peak heights of the interaggregate structure factor may increase with volume fraction by 20 or 30%. This gives a total change in peak height of the intensity of a factor of 2, as observed.

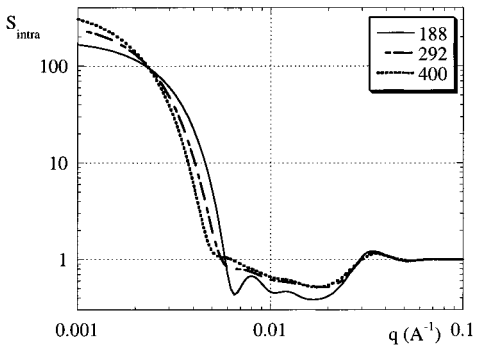

Figure 9. Simulation result of the intraaggregate structure factor $S_{intra}(q)$ as a function of scattering wave vector q in Å^{-1} for $N_{agg} = 188$, $N_{agg} = 292$, and $N_{agg} = 400$.

We do not have any detailed physical model to explain the observed difference in aggregation for beads of different size (B30 and B40), nor of the pH dependence. It is interesting to note that these results differ from what is known from "normal" aggregation, i.e., aggregation of a single component at constant concentration,[42,43] where the primary particle size is of little importance. In our case, we have two components, latex and silica, and monotonically increasing concentrations during drying. The presence of the latex which eventually forms a continuous matrix by film formation allows to stop the aggregation of silica. We think that the competition between the silica aggregation and the solidification of the film is the key: at low pH, for instance, the mutual repulsion between silica beads is reduced, and beads can aggregate before being immobilized. The size dependence is less clear. Theoretical and experimental evidence for higher colloidal stability of bigger spheres exist,[44] but it is questionable whether the small difference in size between B30 and B40 is sufficient to explain the results. Another possibility might be the trivially higher surface charge on the bigger spheres. Here theoretical studies of the pair correlation functions during drying might allow for a deeper understanding.

V. Conclusion

We have reported on the synthesis of a model soft−hard nanocomposite material formed from nanolatex and nanosilica spheres. The physicochemical parameters relevant for the synthesis have been varied systematically, and for each sample a structural analysis by means of small-angle neutron scattering has been performed. Because of important structural changes, the observed SANS spectra are very heterogeneous, and no simple description in terms of some generic fitting function seems feasible. However, it has been possible to identify the main features of the scattering function, and this has lead us to a coherent description of the

scattered intensity of all our samples. As an important result, the evolution of the average number of aggregation could be followed and the close correlation between the parameters of the synthesis of the material and its structure could be confirmed.

As far as theory is concerned, it would be very interesting to have a theoretical description of the nontrivial evolution of the structure with the physicochemical parameters. Another important issue is the modeling of the scattering curves to obtain a more trustworthy estimation of the average number of aggregation.

Acknowledgment. We are indebted to Jean-Christophe Castaing (Rhodia) for the nanolatex and to Akzo Nobel for the silica stock solutions. Interesting discussions with François Boué on reinforcement and help with the D11 scattering experiment are acknowledged.

Appendix A

We describe the polydispersity in size of the silica beads with a log-normal distribution with parameters R_0 and σ:

$$\frac{1}{\sqrt{2\pi}R\sigma}\exp\left(-\frac{1}{2\sigma^2}\ln^2\frac{R}{R_0}\right) \quad \text{(A1)}$$

At low concentrations, the structure factor between beads can be neglected and the scattered intensity written as a sum over the distribution function, eq A1, and the form factor of individual spheres. Several observables, which are of use for the interpretation of the data, are then found to be directly related to various moments of the distribution. These are the low-q limit of the intensity $I_0 = I(q\rightarrow 0)$, the equivalent sphere radius R_{Guinier}, and the Porod radius R_{p}:

$$I_0 = \Phi\Delta\rho_{\mathrm{si-la}}^2\frac{4\pi}{3}\frac{\langle R^6\rangle}{\langle R^3\rangle} = \Phi\Delta\rho_{\mathrm{si-la}}^2\frac{4\pi}{3}R_0{}^3\mathrm{e}^{27\sigma^2/2}$$

$$R_{\mathrm{Guinier}}^2 = \frac{\langle R^8\rangle}{\langle R^6\rangle} = R_0{}^2\mathrm{e}^{14\sigma^2} \quad \text{(A2)}$$

$$R_{\mathrm{p}} = \frac{\langle R^3\rangle}{\langle R^2\rangle} = R_0\mathrm{e}^{5\sigma^2/2}$$

R_{Guinier} is defined as the average sphere radius that yields the same low-q decay as the polydisperse population:

$$I(q) = I_0\left(1 - \frac{q^2R_{\mathrm{Guinier}}^2}{5} + \ldots\right) \quad (q^2R_{\mathrm{Guinier}}^2 < 1) \quad \text{(A3)}$$

R_{p} is defined as the average radius that yields the same specific surface S/V as the polydisperse population:

$$\frac{S}{V} = \frac{3\Phi}{R_{\mathrm{p}}} \quad \text{(A4)}$$

S/V is obtained from the large-q limit of the scattered intensity through the Porod law.[36,45]

Appendix B

We wish to estimate the importance of the population of big aggregates from the limited information contained in the small-q upturn observed in some data sets. In our model we assume (a) a simple functional form for the form factor of big aggregates in order to describe the small-angle upturn, that (b) the plateau is the constant low-q part of the form factor of individual beads, and that (c) both contributions are additive. The intensity at small and intermediate q values then reads

$$I_0 = \Phi(f + (1-f)((N_{\mathrm{agg}} - 1)\mathrm{e}^{q^2R_{\mathrm{g}}{}^2/3} + 1)) \times 5480\ \mathrm{cm}^{-1} \quad \text{(B1)}$$

Here f is the fraction of beads present individually. Their contribution to the scattering, 5480 cm^{-1}, is calculated from the data for B40 given in Table 1 and the first of eqs A2. The form factor of the big aggregates, in the second part of eq B1, is constructed by adding the high-q (constant) and low-q (exponential) behavior. R_{g} is the radius of gyration of the big aggregates. It can be deduced by fitting the data, together with the product of the number of aggregation of the big aggregates N_{agg} and the fraction of beads they contain $(1 - f)$. Better fits of the upturn are obtained with another form factor, a Lorenzian, which is also more appropriate for noncompact structures:

$$I_0 = \Phi\left(f + (1-f)\left(\left(\frac{N_{\mathrm{agg}} - 1}{1 + q^2R_{\mathrm{g}}{}^2/3} + 1\right)\right)\right) \times 5480\ \mathrm{cm}^{-1} \quad \text{(B2)}$$

As the number of aggregation and the size of the aggregate are linked, it is possible to exclude certain combinations on physical grounds, like small N_{agg} and very big sizes. In the absence of ultralow q spectra, however, unique solutions cannot be obtained.

References and Notes

(1) *Science and Technology of Rubber*; Mark, J. E., Erman, B., Eirich, F. R., Eds.; Academic Press: San Diego, CA, 1994.
(2) *Mechanical Properties of Polymers and Composites*; Nielsen, L. E., Landel, R. F., Eds.; Marcel Dekker: New York; 1994.
(3) Edwards, D. C. *J. Mater. Sci.* **1990**, *25*, 4175.
(4) Boonstra, B. B. *Polymer* **1979**, *20*, 691.
(5) Medalia, A. I. *J. Colloid Interface Sci.* **1970**, *32*, 115.
(6) Voet, A. *J. Polym. Sci.: Macromol. Rev.* **1980**, *15*, 327.
(7) Westermann, S.; Kreitschmann, M.; Pyckhout-Hintzen, W.; Richter, D.; Straube, E.; Farago, B.; Goerigk, G *Macromolecules* **1999**, *32*, 5793.
(8) Botti, A.; Pyckhout-Hintzen, W.; Richter, D.; Straube, E.; Urban, V.; Kohlbrecher, J. *Physica B (Amsterdam)* **2000**, *276*, 371.
(9) Nakatani, A. I.; Cen, W.; Schmidt, R. G.; Gordon, G. V.; Han, C. C. *Polymer* **2001**, *42*, 3713.
(10) Heinrich, G.; Vilgis, T. A. *Macromolecules* **1993**, *26*, 1109.
(11) Sharaf, M. A.; Kloczkowski, A.; Mark, J. E. *Comput. Polym. Sci.* **1994**, *4*, 29.
(12) Kloczkowski, A.; Sharaf, M. A.; Mark, J. E. *Chem. Eng. Sci.* **1994**, *49*, 2889.
(13) Vacatello, M. *Macromolecules* **2001**, *34*, 1946.
(14) Vidal, A.; Donnet, J. B. *Prog. Colloid Polym. Sci.* **1987**, *75*, 201.
(15) Payne, A. R. In *Reinforcement of Elastomers*; Kraus, G., Ed.; Interscience Publishers: New York, 1965.
(16) Scott, C.; Ishida, H.; Maurer, F. H. J. *J. Mater. Sci.* **1991**, *26*, 5708.
(17) Maier, P.; Goeritz, D. *Kautsch Gummi Kunstst* **1996**, *49*, 18.
(18) Shang, S. W.; Williams, J. W.; Söderholm, K. J. M. *J. Mater. Sci.* **1992**, *27*, 4949.
(19) Kraus, G. *J. Appl. Polym. Sci., Appl. Polym. Symp.* **1984**, *39*, 75.
(20) Ehrburger-Dolle, F.; Hindermann-Bischoff, M.; Livet, F.; Bley, F.; Rochas, C.; Geissler, E. *Langmuir* **2001**, *17*, 329.
(21) Rieker, T. P.; Misono, S.; Ehrburger-Dolle, F. *Langmuir* **1999**, *15*, 914.
(22) Inoue, T.; Moritani, M.; Hashimoto, T.; Kawai, H. *Macromolecules* **1971**, *4*, 500.

(23) Polmanteer, K. E.; Lenz, C. W. *Rubber Chem. Technol.* **1975**, *48*, 795.
(24) McCarthy, D. W.; Mark, J. E.; Schaefer, D. W. *J. Polym. Sci., Part B* **1998**, *36*, 1167.
(25) McCarthy, D. W.; Mark, J. E.; Clarson, S. J.; Schaefer, D. W. *J. Polym. Sci., Part B* **1998**, 36, 1191.
(26) (a) Rharbi, Y.; Joanicot, M.; Vacher, A.; Cabane, B.; Boué, F. *Europhys. Lett.* **1999**, *46*, 472. (b) Rharbi, Y.; Boué, F.; Joanicot, M.; Cabane, B. *Macromolecules* **1996**, *29*, 4346.
(27) Huber, G.; Vilgis, T. A.; Heinrich, G. *J. Phys.: Condens. Matter* **1996**, L409.
(28) Witten, T. A.; Rubinstein, M.; Colby, R. H. *J. Phys. II* **1993**, *3*, 367.
(29) Ahmed, S.; Jones, F. R. *J. Mater. Sci.* **1990**, *25*, 4933.
(30) Sharaf, M. A.; Kloczkowski, A.; Mark, J. E. *Comput. Theor. Polym. Sci.* **2001**, *11*, 251.
(31) Wang, S.; Mark, J. E. *Macromolecules* **1990**, *23*, 4288.
(32) Winnik, M. A. *Curr. Opin.Colloid Interface Sci.* **1997**, *2*, 192.
(33) Joanicot, M.; Wong, K.; Cabane, B. *Macromolecules* **1996**, *29*, 4976.
(34) Dingenouts, N.; Ballauf, M. *Langmuir* **1999**, *15*, 3283.
(35) Calmettes, P. *J. Phys. IV* **1999**, *9*, 83.
(36) *Neutrons, X-ray and Light Scattering*; Lindner, P., Zemb, Th., Eds.; North-Holland: Amsterdam, 1991.
(37) Lairez, D. *J. Phys. IV* **1999**, *9*, 67.
(38) *Small Angle X-Ray Scattering*; Glatter, O., Kratky, O., Eds.; Academic Press: London, 1982.
(39) *Small-Angle Scattering of X-Rays*; Guinier, A., Fournet, G., Eds.; John Wiley & Sons: New York, 1955.
(40) Oberdisse, J.; Rharbi, Y.; Boué, F. *Comput. Theor. Polym. Sci.* **2000**, *10*, 207.
(41) (a) Hamsy, A.; Vacher, R.; Jullien, R. *Phys. Rev. B* **1994**, *50*, 1305. (b) Hamsy, A.; Anglaret, E.; Foret, M.; Pelous, J.; Jullien, R. *Phys. Rev. B* **1994**, *50*, 6006.
(42) Martin, J. E.; Wilcoxon, J. P.; Schaefer, D.; Odinek, J. *Phys. Rev. A* **1990**, *41*, 4379.
(43) Zhou, Z.; Chu, B. *J. Colloid Interface Sci.* **1991**, *143*, 356.
(44) (a) Behrens, S. H.; Borkovec, M.; Schurtenberger, P. *Langmuir* **1998**, *14*, 1951. (b) Behrens, S. H.; Christl, D. I.; Emmerzael, R.; Schurtenberger, P.; Borkovec, M. *Langmuir* **2000**, *16*, 2566.
(45) Cotton, J. P. *J. Phys. IV* **1999**, *9*, 21.
(46) The small discontinuities in the fits stem from the overlap of different configurations.
(47) This is confirmed by the spectrum of a sample of almost identical composition (B30, $\Phi = 5.0\%$, pH 9.1), which had been mesured on D11 (cf. Figure 2), thus with a higher resolution and larger q range. A small-q upturn is also present.

MA0118419